IOPscience iopscience.iop.org

Home Search Collections Journals About Contact us My IOPscience

Magnetotransport studies of the organic superconductor kappa -(BEDT-TTF)$_2$Cu(NCS)$_2$ under pressure: the relationship between carrier effective mass and critical temperature

This article has been downloaded from IOPscience. Please scroll down to see the full text article.

1994 J. Phys.: Condens. Matter 6 2911

(http://iopscience.iop.org/0953-8984/6/15/013)

View the table of contents for this issue, or go to the journal homepage for more

Download details:
IP Address: 171.66.16.147
The article was downloaded on 12/05/2010 at 18:10

Please note that terms and conditions apply.

J. Phys.: Condens. Matter 6 (1994) 2911–2924. Printed in the UK

Magnetotransport studies of the organic superconductor κ-(BEDT–TTF)$_2$Cu(NCS)$_2$ under pressure: the relationship between carrier effective mass and critical temperature

J Caulfield†, W Lubczynski†§, F L Pratt†¶, J Singleton†, D Y K Ko†, W Hayes†, M Kurmoo‡ and P Day‡

† Physics Department, University of Oxford, Clarendon Laboratory, Parks Road, Oxford OX1 3PU, UK

‡ The Royal Institution, 21 Albermarle Street, London W1X 4BS, UK

Received 14 January 1994

Abstract. Magnetotransport measurements have been carried out on the organic superconductor κ-(BEDT–TTF)$_2$Cu(NCS)$_2$ at temperatures down to 500 mK and in hydrostatic pressures up to 16.3 kbar. The observation of Shubnikov–de Haas and magnetic breakdown oscillations has allowed the pressure dependences of the area of the closed pocket of the Fermi surface and the carrier effective masses to be deduced and compared with simultaneous measurements of the superconducting critical temperature T_c. The effective mass measured by the temperature dependence of the Shubnikov–de Haas oscillations is found to fall rapidly with increasing pressure up to a critical pressure $P_c \simeq 5$ kbar. Above P_c a much weaker pressure dependence is observed; T_c also falls rapidly with pressure from 10.4 K at ambient pressure to zero at around P_c. This strongly suggests that the enhanced effective mass and the superconducting behaviour are directly connected in this organic superconductor.

A simplified model of the bandstructure of κ-(BEDT–TTF)$_2$Cu(NCS)$_2$ has been used to derive the bare band masses of the electrons from optical data. Comparisons of these parameters with cyclotron resonance data and the effective masses measured in the present experiments indicate that the greater part of the enhancement of the effective mass necessary for superconductivity in this material is due to quasiparticle interactions, with the electron–phonon interactions playing a secondary role. The dependence of T_c on the effective mass may be fitted satisfactorily to a suitably parametrized weak-coupling BCS expression, although this cannot be taken as a definitive proof of the nature of superconductivity in organic conductors.

1. Introduction

The well separated molecular orbitals and the layered structural arrangements in BEDT–TTF charge transfer salts [1]‖ lead to relatively simple two-dimensional Fermi surface topologies, making the salts ideal for the study of the relationship between bandstructure and electronic properties such as superconductivity. In this context κ-(BEDT–TTF)$_2$Cu(NCS)$_2$, a superconductor with a critical temperature $T_c = 10.4$ K, is an excellent model system. Bandstructure calculations using the room temperature crystal parameters yield a rather simple Fermi surface (see inset to figure 1) consisting of a quasi-two-dimensional (Q2D) hole pocket plus a quasi-one-dimensional (Q1D) electron section [2]. Furthermore, as will

§ Permanent address: Department of Solid State Physics, 41-800 Zabrze, Kalwalca 3, Poland.

¶ Current address: Institute for Materials Research, Tohoku University, Katahira 2-1-1, Sendai 980, Japan.

‖ BEDT–TTF is bis(ethylenedithio)tetrathiofulvalene, sometimes abbreviated to ET.

0953-8984/94/152911+14$19.50 © 1994 IOP Publishing Ltd

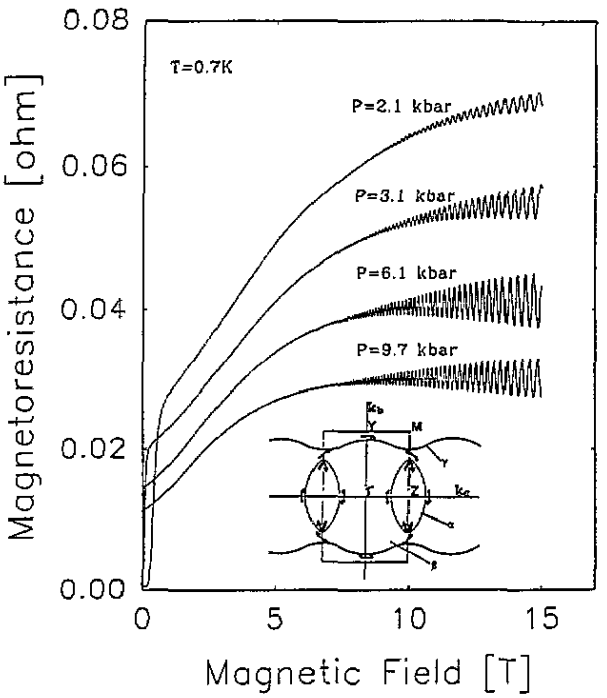

Figure 1. Magnetoresistance of κ-(BEDT–TTF)$_2$Cu(NCS)$_2$ at 0.7 K (magnetic field applied perpendicular to the conducting planes) for four different pressures. The inset shows the Brillouin zone, Fermi surface and α and β orbits (after [6]).

be seen below, excellent crystals of the material are available, so that phenomena such as the Shubnikov–de Haas effect may be readily observed, enabling the Fermi surface topology to be measured accurately.

One of the most striking features of κ-(BEDT–TTF)$_2$Cu(NCS)$_2$ is the rapid decrease of its superconducting T_c with increasing hydrostatic pressure ($\sim -3\,\mathrm{K\,kbar^{-1}}$) [3, 4], which led to successful proposals for raising the T_c accessible in BEDT–TTF salts using chemical synthesis [5] (although there was some controversy over the exact pressure dependence of T_c at very low pressures [4]). The study in this paper was motivated by the opportunity to vary the superconducting properties using pressure and to observe simultaneously bandstructure parameters such as the carrier effective mass and Fermi surface pocket area using the Shubnikov–de Haas effect. Thus the bandstructure and quasiparticle properties which determine the superconducting behaviour can be deduced. The carrier effective mass measured by the Shubnikov–de Haas effect is found to fall rapidly with increasing pressure in the region below a critical pressure $P_c \sim 5$ kbar. Above P_c a much weaker pressure dependence is observed. The superconducting T_c also falls rapidly with pressure, extrapolating to zero around P_c. This strongly suggests that the enhancement of the effective mass and the superconducting transition are directly related in this organic superconductor.

This paper is organized as follows. The experimental arrangements and data obtained are described in sections 2 and 3. To assist in the understanding of the effects of various interactions on the carriers in κ-(BEDT–TTF)$_2$Cu(NCS)$_2$ a simple model of the bandstructure is derived in section 4.1 and used to obtain the variations of the Fermi surface shape with pressure and an estimate of the bare band mass of the

electrons. The effects of electron–phonon and quasiparticle interactions in renormalizing the effective masses are discussed in section 4.2, and the pressure dependence of T_c and the prerequisites for superconductivity in BEDT–TTF salts are covered in section 4.3. A summary is given in section 5.

2. Experimental

High-purity single crystals of κ-(BEDT–TTF)$_2$Cu(NCS)$_2$ were grown by electrocrystallization of BEDT–TTF in distilled 1,1,2-trichloroethane and 10% ethanol using KSCN/CuSCN/18 Crown 6 as the source of the anion; the crystals are generally small ($1 \times 1 \times 0.1\,mm^3$) black platelets, with the plane of the plate corresponding to the highly conducting 2D layers. Electrical contacts were made with silver paste to evaporated gold pads on both platelet faces, resulting in contact resistances of less than 10 Ω. Standard four-wire AC techniques (5–150 Hz), with the current applied perpendicular to the sample 2D planes, were used for all measurements. To avoid sample heating, currents were generally 0.2–20 μA. Magnetoresistance experiments under hydrostatic pressure were carried out using a non-magnetic clamp cell filled with a petroleum spirit medium providing pressures up to 16.5 kbar at helium temperatures. Pressure was applied at room temperature and then the cell was placed in a ^{3}He cryostat providing temperatures down to 500 mK in a 17 T superconducting magnet; cooling from room temperature to 4.2 K was accomplished over a period of around 12 h, to ensure that the pressure was ideally hydrostatic at low temperatures. The temperature of the sample could be varied between 500 mK and 15 K and was measured using calibrated ruthenium oxide and carbon sensors, and the pressure in the cell at all temperatures was monitored using the resistance of Manganin wire with a known pressure and temperature coefficient.

3. Experimental results

3.1. Magnetoresistance data

The magnetoresistance of κ-(BEDT–TTF)$_2$Cu(NCS)$_2$ at 0.7 K is shown for a number of hydrostatic pressures in figure 1. The normal-state conductivity of the sample increases with pressure and the upper critical field H_{c2}, observed as a steep drop in resistance to zero, decreases sharply. A series of Shubnikov–de Haas oscillations is observed in the magnetoresistance, and both the amplitude and the frequency of the oscillations are visibly affected by pressure. These oscillations correspond to k-space orbits around the Q2D hole pocket of the Fermi surface (inset of figure 1) [2]; in common with other authors [6, 7], we shall refer to this as the α orbit for convenience. As the pressure is raised further (figure 2), a second series of oscillations with a higher frequency is observed in the magnetoresistance, superimposed on the oscillations due to the α orbit. Similar high-frequency oscillations have been observed between 20–25 T at ambient pressure, and are attributed to magnetic breakdown [6–8]. Magnetic breakdown is due to electrons tunnelling between states of equal energy in adjacent sections of Fermi surface, thus describing a larger k-space orbit [9]. The inset in figure 1 indicates the primary breakdown orbit (labelled the β orbit) in κ-(BEDT–TTF)$_2$Cu(NCS)$_2$ around the outer edges of both the Q2D and the Q1D Fermi surface sections. The magnetic breakdown oscillation amplitude increases sharply with increasing pressure (figure 2).

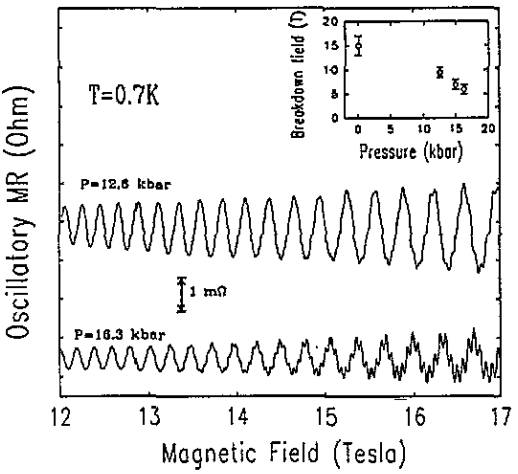

Figure 2. The oscillatory part of the magnetoresistance above 12 T at 0.7 K (magnetic field applied perpendicular to the conducting planes) at two different pressures. The inset shows the characteristic breakdown field B_0 as a function of pressure (see section 3.2; ambient pressure point from [8]).

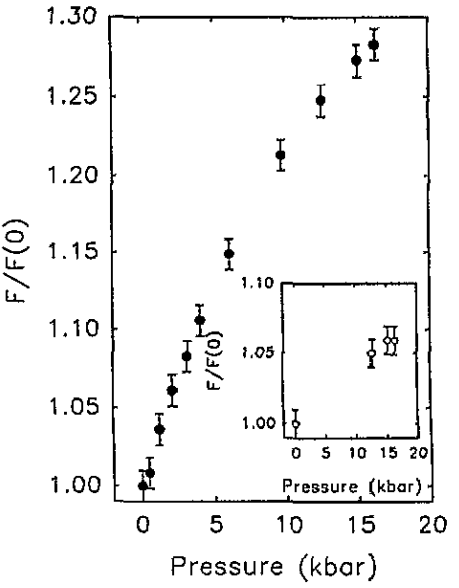

Figure 3. The primary Shubnikov–de Haas oscillation frequency F_α normalized to the ambient pressure value as a function of pressure. The inset shows the breakdown frequency F_β, normalized to the ambient pressure value, against pressure (ambient pressure point taken from [8]). The latter frequency corresponds to the full Brillouin zone area.

3.2. Fermi surface topology and effective masses

Data similar to those in figures 1 and 2 were Fourier transformed in order to obtain the frequencies of the Shubnikov–de Haas and magnetic breakdown oscillations as a function of pressure; the results of this process are shown in figure 3. The measured α-orbit Shubnikov-de Haas frequency F_α increases rapidly from an ambient pressure value of 600 ± 5 T to 775 ± 5 T at 16.3 kbar. As F_α is directly proportional to the k-space area S_α of the α orbit, this indicates that the Q2D section of the Fermi surface has increased in area by around 30%. By contrast, the frequency of the β orbit (3920 ± 10 T at ambient pressure) increases by only 6% to 4182 ± 10 T over the same pressure range (figure 3, inset; the ambient pressure point is taken from [8]). This result is not unexpected, as the band filling in κ-(BEDT–TTF)$_2$Cu(NCS)$_2$ means that the β orbit has the same area as the first Brillouin zone (S_{BZ}) [2, 6–8] so that the slow increase merely reflects the compressibility of the material [10].

The effective masses associated with the α and β orbits were derived by fitting the temperature dependence of the Shubnikov–de Haas and magnetic breakdown oscillation amplitudes, measured in the temperature range 0.5–5 K at each pressure, to the Lifschitz–Kosevich formula [9, 11]. Ignoring the spin splitting, the field (B) and temperature (T) dependence of the amplitude of the first harmonic of the oscillations is given by

$$A = \frac{A_0[T \exp(-L\mu T_D/B)\cos(2\pi F/B + \Psi)]}{\sqrt{B}\sinh(L\mu T/B)} \qquad (1)$$

where A_0 is a constant, $L = 2\pi^2 m_e k_B/eh$, Ψ is an arbitrary phase, T_D is the Dingle temperature and $\mu = m^*/m_e$. As above, F is the frequency of the oscillations. The measured variation of both effective masses with pressure is shown in figure 4. At ambient pressure, $m_\alpha^* = 3.5 \pm 0.1 m_e$, in good agreement with previous measurements [6–8]. The pressure dependence of m_α^* exhibits two distinct regimes; below a critical pressure P_c , m_α^* decreases approximately linearly with pressure at a rate of $dm_\alpha^*/dP = -0.33 m_e\,\mathrm{kbar}^{-1}$, whereas above P_c it decreases at a much lower rate of $\sim -0.04 m_e\,\mathrm{kbar}^{-1}$ to $m_\alpha^* = 1.4 \pm 0.1 m_e$ at 16.3 kbar. The Dingle temperature T_D is difficult to measure accurately but it is found to be ~ 0.5 K and independent of pressure within the experimental error. Within the restricted data set available, the effective mass of the magnetic breakdown β orbit, m_β^*, appears to exhibit a similar pressure dependence to m_α^*, initially falling rapidly from an ambient pressure value of $m_\beta^* = 6.5 \pm 0.1 m_e$ [8] and then decreasing more slowly ($m_\beta^* = 3.0 \pm 0.1 m_e$ at 12.6 kbar and $2.7 \pm 0.1 m_e$ at 16.3 kbar (figure 4).

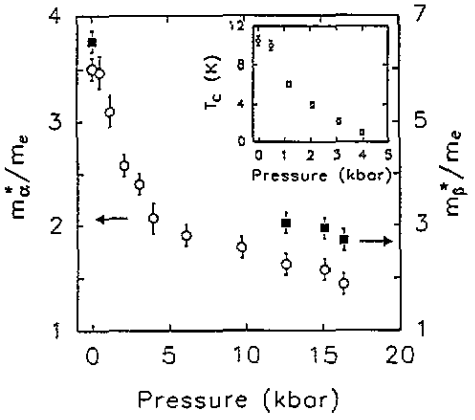

Figure 4. The effective masses of the α orbit (open circles, left-hand vertical scale) and β orbit (full squares, right-hand vertical scale) as a function of pressure. The inset shows the superconducting T_c against pressure.

The small energy gap E_g between the two bands responsible for the Q1D and Q2D sections of Fermi surface [2, 5, 10] may be deduced from the field dependence of the oscillatory component of the magnetoresistance using the Lifshitz–Kosevich formula (1) [9] and the coupled network magnetic breakdown model [12]. This was first applied to κ-(BEDT–TTF)$_2$Cu(NCS)$_2$ by Sasaki and co-workers [6]. As mentioned above, electron tunnelling can occur at the Brillouin zone boundary between neighbouring sections of the Fermi surface (figure 1, inset) with a probability given by

$$P = \exp\left(-\frac{\pi E_g^2}{4\hbar\omega_c \sin(2\theta) E_F}\right) \equiv \exp(-B_0/B) \tag{2}$$

where $\omega_c = eB/m^*$, 2θ is the Bragg reflection angle and $B_0 \equiv \pi m^* E_g^2/4e\hbar \sin(2\theta) E_F$. When more than one frequency of Shubnikov–de Haas oscillation is present, the overall oscillatory component of the magnetoresistance is given by a sum of amplitudes from the Lifshitz–Kosevich formulae for each possible closed orbit. The coupled network model [12] shows that the amplitude of every term concerned is weighted by a 'breakdown reduction factor', $R_b = (ip)^{n_1} q^{n_2}$, where breakdown probability $P = |p|^2 = 1 - Q$, and $Q = |q|^2$. The integers n_1 and n_2 are the number of points at which breakdown occurs and the number of Bragg reflection points respectively. In the case of the closed hole pocket (α orbit) $n_1 = 0$

and $n_2 = 2$, and for the magnetic breakdown β orbit $n_1 = 4$ and $n_2 = 0$. Therefore the total amplitude can be described by

$$A_{\text{tot}} = R_{\text{b},\alpha} A_\alpha + R_{\text{b},\beta} A_\beta \tag{3}$$

where $R_{\text{b},\alpha} = q^2 = 1 - P$ and $R_{\text{b},\beta} = (\text{i}p)^4 = P^2$. Using the experimental values of the effective masses, Dingle temperature and Shubnikov–de Haas oscillation frequencies, the field dependence of the oscillatory magnetoresistance has been simulated using (1)–(3) with the breakdown field B_0 as the only variable parameter. The breakdown field as a function of pressure is shown in the inset to figure 2. At ambient pressure, the energy gap E_g is estimated to be 55 ± 5 K, in agreement with previous measurements [6]. This is obtained from the fitted value $B_0 = 15 \pm 1$ T [8] with $2\theta = \pi/2$, $E_F = 740 \pm 100$ K [6], $m_\beta^* = 6.5 \pm 0.1 m_e$ and $k_F^2 \pi = 3.63 \times 10^{15}\,\text{cm}^{-2}$; the latter two parameters were measured in magnetic fields of up to 25 T where magnetic breakdown was clearly observed [8]. A linear extrapolation of the pressure dependence of the breakdown field suggests closure of the energy gap at around 25 kbar.

3.3. Superconducting properties under pressure

The superconducting T_c (midpoint) of κ-(BEDT–TTF)$_2$Cu(NCS)$_2$ was also measured at each pressure; the results are shown as an inset to figure 4. The data are consistent with most of the previous reports [3], giving an initial pressure coefficient of $\sim -3\,\text{K kbar}^{-1}$, and there is no evidence for a low-pressure plateau extending up to several kbar as reported by some authors [4]. The superconductivity is fully suppressed above 5 kbar. Note that this pressure is the same as P_c, the crossover point in the pressure dependence of the effective mass, to within experimental errors. The relationship between the pressure dependence of the effective mass and T_c will be considered further below.

4. Discussion

4.1. The Fermi surface: an effective dimer model

The intermolecular overlap integrals and the corresponding tight-binding bandstructure and Fermi surface of κ-(BEDT–TTF)$_2$Cu(NCS)$_2$ have been calculated by a number of workers [2, 5, 10]. The Fermi surface may be viewed as a cylinder with a slightly elliptical cross section (figure 1, inset) which crosses the Brillouin zone boundary in the c^* direction. The unit cell contains two dimers [2, 10]; a slight inequivalence of the two molecules in each dimer causes a small energy gap to be present at the zone boundary, splitting the Fermi surface into open (Q1D) and closed (Q2D) sections. The calculated bandstructure is therefore in reasonable qualitative agreement with experimental data and the predicted area of the Q2D Fermi surface pocket [2, 5, 10] is very close to that given by the α-orbit Shubnikov–de Haas oscillation frequency [6–8, 13, 14]. Furthermore, the observation of magnetic breakdown confirms the existence of the small energy gap giving rise to the two sections of Fermi surface [6–8]. However, the pressure-dependent measurements reported in this paper potentially allow rather stringent tests of the bandstructure calculations to be carried out. The alterations in the overlap integrals and bandstructure caused by changing the pressure can in principle be predicted from structural data recorded under the same conditions. The crystal structure has been measured at low temperature under ambient pressure and also at room temperature under pressures of up to 7 kbar [10]. The transfer

integrals were calculated to increase with pressure [10], as would be expected from the increasing overlap of the molecular orbitals on adjacent molecules. However, the energy gap at the ZM Brillouin zone boundary was calculated to increase with pressure, with a corresponding reduction in the size of the closed orbit. Both of these predictions are contrary to our experimental findings. The Shubnikov–de Haas oscillations described in sections 3.1 and 3.2 indicate that the Q2D section of the Fermi surface increases in area by around 30% between ambient pressure and 16.3 kbar, whereas the area of the whole Fermi surface, as measured by the frequency of the β orbit, increases by only 6% over the same pressure range (figure 3). The magnetic breakdown oscillations (figure 2) indicate that the energy gap decreases with increasing pressure. It must be concluded that whilst present calculations of the bandstructure of κ-(BEDT–TTF)$_2$Cu(NCS)$_2$ provide a reasonably correct general picture of the Fermi surface, problems arise when the models are applied to the pressure dependence of the band parameters. The difficulty almost certainly results from inconsistencies between the conditions under which the structural data [10] and the results in this work were recorded. It will therefore be necessary to perform x-ray crystallography measurements at both low temperatures and a range of hydrostatic pressures before further quantitative comparisons between detailed bandstructure calculations and these experiments can be made.

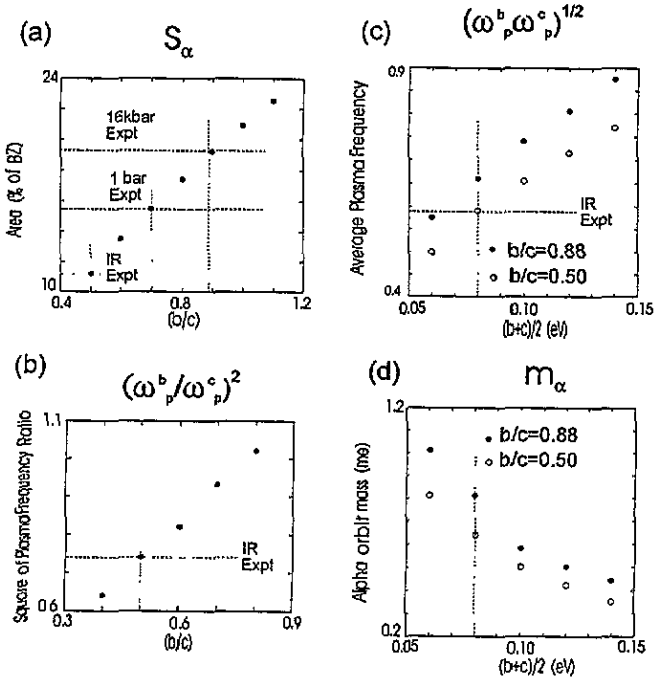

Figure 5. Various Fermi surface properties calculated using the effective dimer model as a function of the transfer integrals b and c (see text). (*a*) The Q2D hole pocket area (α orbit); (*b*) plasma frequency ratio; (*c*) the average plasma frequency, and (*d*) the α orbit band mass. The dotted curves indicate experimental results taken from magnetotransport data in this paper (1 bar expt, 16 kbar expt) and from optical data in [17] (IR expt) used to define b and c (see section 4.1 and table 1).

In the absence of structural data which would allow the use of more sophisticated models, we shall use a simplified form of bandstructure calculation that takes account of

the highly dimerized nature of the structure [2, 5] in order to describe and understand the pressure-induced changes in the Fermi surface. We refer to this calculation as the effective dimer model; a similar approach was used by Tamura and co-workers [15] to analyse the reflectivity of κ-(BEDT–TTF)$_2$I$_3$. The basic unit for the tight-binding calculations is taken to be the dimer with its antibonding dimer orbital as the basis wavefunction. There are thus two dimers per unit cell and only three overlap integrals, one, b, corresponding to interdimer overlap in the b direction, and c_1 and c_2 which relate to the overlap in the c direction; these latter two are slightly different due to the non-symmetrical position of the dimer. The energy bands are calculated to be

$$E = 2b\cos k_b \pm [2(c_1^2 + c_2^2 + 2c_1c_2\cos k_c)(1 + \cos k_b)]^{1/2} \tag{4}$$

where the k vectors are in reduced units ($|k_b|$, $|k_c| = \pi$ on the respective Brillouin zone boundaries). Along the ZM zone boundary $\cos k_c = -1$ and furthermore $\cos k_b \sim -0.5$ where the Fermi surface crosses the zone boundary (figure 1, inset). The energy gap at this point thus becomes $\Delta E \simeq 2(c_1 - c_2)$ and this is measured directly from the magnetic breakdown oscillations ([6–8] and figure 2) to be $\simeq 5$ meV at ambient pressure, and ~ 1 meV at 16 kbar. This splitting is small compared to the size of the overlap integrals so that $c_1 \simeq c_2 \simeq c$. Consequently the *shape* of the Fermi surface depends almost entirely on the ratio of the transfer integrals b and c. Figures 5(a) and 5(b) show the dependence of various parameters on b/c. Using the experimental α-orbit Shubnikov–de Haas oscillation frequencies to give the Q2D hole pocket area, b/c is deduced to be 0.70 at ambient pressure and 0.88 at 16.3 kbar (figure 5(a)). Figure 6 shows the consequent calculated shape of the Fermi surface at these two pressures. An increase in pressure appears to result in the transfer integrals becoming more similar.

It is also possible to estimate the ratio of the transfer integrals from polarized infrared reflectance measurements. Care must be taken to separate the intraband from the interband contributions observed in the optical reflectivity data in order to obtain the true intraband plasma frequency. This procedure was carried out at room temperature by Sugano and co-workers [16], giving the values $\omega_p^b = 0.61$ eV and $\omega_p^c = 0.71$ eV for $E//b$ and $E//c$ respectively, and at 25 K by Ugawa and co-workers [17], who reported values $\omega_p^b = 0.55$ eV and $\omega_p^c = 0.64$ eV. Note that the ratio of the plasma frequencies $(\omega_p^b/\omega_p^c) = 0.86$ is the same in both measurements. The ratio of the intraband plasma frequencies calculated using the bandstructure of (4) is shown as a function of b/c in figure 5(b); $b/c = 0.50$ is necessary to give the observed plasma frequency ratio. This is significantly lower than the values obtained from the Shubnikov–de Haas oscillations, and figure 6 compares the Fermi surface shapes derived using the effective dimer model from the plasma frequency ratios (i.e. optical data) and the magnetotransport data at 0 kbar and 16.3 kbar. The reasons for the differences between the Fermi surfaces derived from optical and Shubnikov–de Haas data will be discussed in the following section.

So far only the dimensionless ratio b/c has been determined from the data. In order to fit the absolute values of the plasma frequencies and the variation of the carrier effective masses with pressure, the sizes of the parameters b and c must be determined. A relatively straightforward estimation of b and c may be made by fitting the low-temperature optical data of Ugawa and co-workers [17] to the effective dimer model (figure 5(c)); as the ratio of b/c has already been determined from the plasma frequency ratio (figure 5(b)), it is sufficient to find $(b + c)/2$. The parameters thus deduced are shown in the first line of table 1 and compared with those derived from the magnetotransport data. Using these parameters, the bare band mass of the Q2D hole pocket (corresponding to the α orbit) may estimated to be

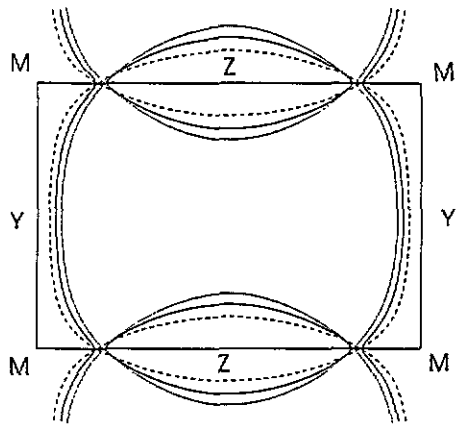

Figure 6. The Fermi surface of κ-(BEDT–TTF)$_2$Cu(NCS)$_2$ calculated using the effective dimer model bandstructure fitted to magnetotransport data at 0 kbar (full curve) and 16.3 kbar (dotted curve) and to optical data [17] (broken curve). The k vectors are in reduced units and the Brillouin zone has been kept the same size for each Fermi surface for clarity. See table 1 for the parameters used.

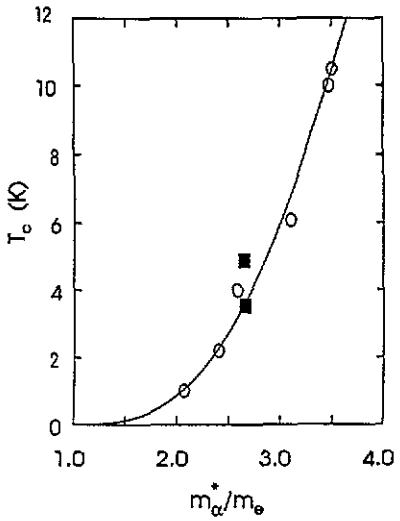

Figure 7. The relationship between the effective mass of the α orbit and the superconducting T_c for κ-(BEDT–TTF)$_2$Cu(NCS)$_2$. The open circles are from the pressure-dependent magnetotransport data in this paper and the full squares are data for other superconducting κ-phase salts at ambient pressure (upper point κ-(BEDT–TTF)$_2$Ag(CN)$_2$ [26], lower point κ-(BEDT–TTF)$_2$I$_3$ [27]. The fitted curve is derived using a weak-coupling BCS formula (5) and parameters given in section 4.3.

$m_{b\alpha} \simeq 0.64m_e$ (figure 5(d)). A similar procedure gives a bare band mass corresponding to the β orbit to be $m_{b\beta} \simeq 1.27m_e$. These are much smaller than the effective masses observed in the experiments, and so before proceeding it is necessary to clarify the meaning of the effective masses measured using the Shubnikov–de Haas effect and optical experiments.

Table 1. Comparison of the parameters of the effective dimer model and the corresponding calculated Fermi surface properties estimated from fitting to optical (Opt.) [17] and magnetotransport data (this work). The resulting calculated Fermi surfaces are shown in Figure 5.

	b (eV)	c (eV)	b/c	E_g (meV)	$\frac{S_\alpha}{S_{BZ}}$ (%)	ω_p^b (eV)	ω_p^c (eV)	ω_p^b/ω_p^c	$m_{b\alpha}$	$m_{b\beta}$
Opt.	0.060	0.12	0.50		11.4	0.55	0.64	0.86	0.64	1.27
0 kbar			0.70	5	15.5			0.96		
16 kbar			0.88	~ 1	18.7			1.09		

4.2. Ambient pressure effective masses and the influence of many-body effects

It has been clear for some time that the effective masses of carriers in BEDT–TTF charge-transfer salts measured using the Shubnikov–de Haas and de Haas–van Alphen effects are much larger than those predicted by bandstructure calculations [13, 14, 18], leading to the suggestion that many-body effects are of great importance [13, 18]. Within the

theory of interacting fermions a number of quasiparticle 'masses' can be defined, reflecting the differing dynamical behaviour involved in various physical properties [19,20]; the differences between these masses provide important information about the many-body interactions in the system. Perhaps the simplest is the bare band mass m_b, which is derived from single-particle bandstructure calculations. This is very close in size to the optical mass m_{opt}, which can be experimentally probed by an optical measurement of the intraband plasma response [19,20].

Two further quasiparticle masses are important in the context of the experiments reported in this paper. The effective mass m^* occurs in the thermodynamic density of states, and may crudely be thought of as arising from a quasiparticle displacing other quasiparticles as it moves through a medium. The backflow of quasiparticles leads to a contribution to the effective mass m^*. The dynamical mass m_λ is the mass which would be observed in the absence of quasiparticle interactions, and the ratio of the two quantities is $m^*/m_\lambda = (1 + F_1^s/3)$, where F_1^s is the $l = 1$ Fermi liquid parameter [19]. The dynamical mass therefore represents the band mass renormalized only by electron–phonon interactions, whereas m^* is renormalized by both quasiparticle interactions and electron–phonon interactions. The ratio of the masses m_λ/m_b is the electron–phonon enhancement factor $1 + \lambda$. The dynamical mass and effective mass may be measured using low-energy experimental probes; the temperature dependence of phenomena such as the Shubnikov–de Haas and de Haas–van Alphen effects determines the effective mass m^* whereas a microwave cyclotron resonance experiment measures m_λ [18–20].

Although electron–phonon interactions lead to a renormalization of the band mass to give the dynamical mass, they do not change the shape of the Fermi surface. However, quasiparticle interactions can change the shape of the Fermi surface but according to Luttinger's theorem [21] the volume of the Fermi surface should remain unchanged. This suggests a possible reason for the difference in Fermi surface shapes deduced from the Shubnikov–de Haas and optical measurements (figure 6); the 'optical Fermi surface' represents the shape in the absence of quasiparticle interactions whereas those determined from the magnetotransport data include the effects of those interactions.

Table 2. Comparison of the various quasiparticle masses in κ-(BEDT–TTF)$_2$Cu(NCS)$_2$.

Parameter	α orbit (m_e)	β orbit (m_e)	Note/Reference
m_b	0.64	1.27	Fitted to optical data [17] using *effective dimer model (this paper)*
m_λ	1.18		Cyclotron resonance [22]
m^*	3.5 ± 0.1	6.5 ± 0.1	Measured using Shubnikov–de Haas effect (this paper)
m^*/m_b	5.5	5.1	

The various quasiparticle masses which can be deduced from ambient pressure experimental data are shown in table 2. Microwave magneto-optical studies have been performed on κ-(BEDT–TTF)$_2$Cu(NCS)$_2$ at ambient pressure by Hill and co-workers [22]. The features observed were interpreted as cyclotron resonances due to the Q2D hole pocket (i.e. α orbit) and a value of $m_{\lambda\alpha} = 1.18m_e$ was obtained [22]. Using $m_{b\alpha} \simeq 0.64m_e$, obtained above by fitting the low-temperature optical data using the effective dimer model (table 1), the value of $m_{\lambda\alpha}/m_{b\alpha} = 1 + \lambda$ implies that $\lambda \simeq 0.7$–0.8. This is similar in size to, but larger than, estimates of a total intramolecular $\lambda \simeq 0.3$–0.5 for various BEDT–TTF

salts derived by analysis of the frequencies of the phonons observed in infrared and Raman spectroscopy [23] and by thermodynamical approaches using the Gruneisen parameters and BCS theory [24]. It is also typical of λ values proposed for other similar organic radical salts [5, 23, 25]. Note that small shifts in $m_{b\alpha}$ would result in comparatively large changes in λ.

A value of $m_\alpha^* = 3.5m_e$ was measured above using the temperature dependence of the Shubnikov–de Haas effect at ambient pressure (figure 4). This represents an enhancement of a factor of about three over $m_{\lambda\alpha}$. The quasiparticle interactions therefore represent a rather larger renormalization of the quasiparticle mass than do the electron–phonon interactions. No cyclotron resonance data corresponding to the β orbit has yet been observed. However, the ratios $m_\alpha^*/m_{b\alpha}$ and $m_\beta^*/m_{b\beta}$ are similar (table 2), indicating that the overall renormalization of the bare band mass is relatively uniform over the whole Fermi surface.

In summary, the effects of many-body interactions appear to be very important in renormalizing the bare bandstructure masses of the quasiparticles in κ-(BEDT–TTF)$_2$Cu(NCS)$_2$ at ambient pressure. The largest contribution comes from the quasiparticle interactions, which renormalize the dynamical mass by a factor of about three.

4.3. The effect of pressure on the effective masses and superconducting behaviour

Figure 4 shows the pressure dependence of the effective mass of the α orbit, m_α^*. Two distinct regions are observed. Above a pressure P_c the masses lie approximately on a straight line with a low value of dm_α^*/dP, which extrapolates back to $m'_{\alpha 0} = 2.1m_e$ at zero pressure, whereas below P_c the data lie on a line with dm_α^*/dP some eight times larger, which extrapolates to $m_{\alpha 0}^* = 3.5m_e$ at zero pressure. Qualitatively similar changes also occur in the effective mass of the β orbit. The variation of the superconducting critical temperature with pressure and its disappearance at P_c (figure 4, inset) appears to be connected with the rapid variation of the effective mass in this region.

Any model of superconductivity should potentially allow one to relate the critical temperature to the effective mass. For instance, in the weak-coupling BCS scheme the superconducting transition temperature is given by

$$T_c = 1.13\Theta \exp[-1/(\lambda - \mu^*)] \tag{5}$$

where λ is the electron–phonon coupling constant and μ^* is the Coulomb pseudopotential, representing the effective repulsion between the electrons in a Cooper pair [5, 25]. Θ is typically the Debye temperature and sets the energy scale of the interaction. The electron–phonon coupling constant is proportional to the density of states at the Fermi surface, which is in turn proportional to the effective mass. Figure 4 shows that the effective mass varies rapidly at low pressures, and so the strongest effect influencing T_c is likely to be the variation in the density of states at the Fermi energy. In figure 7, the $T_c(P)$ data are modelled using equation (5) with $\lambda(P) = \lambda(0)m_\alpha^*(P)/m_\alpha^*(0)$ and the other parameters held constant†. With $\lambda(0) = 0.30 \pm 0.03$, $\mu^* = 0$ (i.e. $\mu^* << \lambda$) and $\Theta = 270 \pm 10$ K, a good fit to the transition temperature as a function of the effective mass can be obtained (see figure 7). Ambient pressure data from two other κ-phase BEDT–TTF salts [26, 27] are also included in figure 7 and are fitted well by the curve.

† Strictly $m_\beta^*(P)$, which represents the effective mass of the whole Fermi surface, should be used to scale λ. However, the pressure dependences of m_α^* and m_β^* are very similar when conditions permit m_β^* to be measured (figure 4), and the ratios $m_\alpha^*/m_{b\alpha}$ and $m_\beta^*/m_{b\beta}$ are almost the same (table 2), indicating that the overall renormalization of the bare band mass is relatively uniform over the whole Fermi surface. The pressure dependences of $m_\alpha^*(P)/m_\alpha^*(0)$ and $m_\beta^*(P)/m_\beta^*(0)$ are therefore taken to be identical.

Whilst the $T_c(P)$ against $m_\alpha^*(P)$ curve in figure 7 fits the experimental results well, equation (5) must be seen as merely a convenient parametrization of the data rather than a test of the nature of superconductivity in organic molecular metals. Although a strong-coupling BCS expression cannot be made to fit the data well [28], several points suggest that the applicability of weak coupling BCS theory to κ-(BEDT–TTF)$_2$Cu(NCS)$_2$ remains an open question; for example, the fitted value of $\mu^* = 0$ contradicts expectations for a strongly correlated electron system†, and the Debye temperature of κ-(BEDT–TTF)$_2$Cu(NCS)$_2$ obtained from specific heat measurements is around 215 K [29]. It is, however, clear that the experimental variation in T_c corresponds directly to changes in the electronic density of states associated with the changes in effective mass.

It therefore seems that large effective masses are a prerequisite for superconductivity in BEDT–TTF salts and, following the discussion in section 4.2, that the mechanisms primarily responsible for producing the effective mass enhancement are due to the interactions between quasiparticles, with the electron–phonon interactions playing a smaller role. The effects of quasiparticle interactions are expected to depend strongly on the bandwidth (see, for example, [30]), being larger in general for narrower bands. An increase in the hydrostatic pressure will bring the BEDT–TTF molecules closer together and hence broaden the bands. The initial strong decrease in effective mass with pressure could therefore represent the suppression of a component of the quasiparticle interactions which depends critically on the bandwidth. Above P_c the more gentle decrease of the experimental effective masses with pressure may well merely reflect the increasing bandwidth and the concomitant decrease in the bare band masses.

5. Summary

Magnetotransport measurements have been carried out on the organic superconductor κ-(BEDT–TTF)$_2$Cu(NCS)$_2$ at temperatures down to 500 mK and in hydrostatic pressures up to 16.3 kbar. The observation of Shubnikov–de Haas and magnetic breakdown oscillations has allowed the pressure dependences of the area of the closed pocket of the Fermi surface and the carrier effective masses to be deduced and compared with simultaneous measurements of the superconducting critical temperature T_c. The effective mass measured by the temperature dependence of the Shubnikov-de Haas oscillations is found to fall rapidly with increasing pressure up to a critical pressure $P_c \simeq 5$ kbar. Above P_c a much weaker pressure dependence is observed. T_c also falls rapidly with pressure from 10.4 K at ambient pressure to zero at around P_c. This strongly suggests that the enhanced effective mass and the superconducting transition temperature are directly connected in this organic superconductor.

A simplified model of the bandstructure of κ-(BEDT–TTF)$_2$Cu(NCS)$_2$ has been used to derive the bare band masses of the electrons from optical data. Comparisons of these parameters with cyclotron resonance data and the effective masses measured in the present experiments indicate that the greater part of the enhancement of the effective mass necessary for superconductivity in this material is due to quasiparticle interactions, with the electron–phonon interactions playing a secondary role. The quasiparticle interactions appear to depend critically on the bandwidth, being considerably suppressed by the application of 5 kbar. An understanding of the nature of these interactions is an important question for further experimental and theoretical studies.

† Professor Maki has suggested that μ^* would be zero for the case of d-wave pairing. We are grateful to him for communicating this point.

Acknowledgments

This work is supported by the Science and Engineering Research Council (UK) and by the European Community. WL is grateful to the Royal Society for the provision of a Visiting Fellowship for the duration of his stay in Oxford. We should also like to thank Dennis Rawlings and Terry Holliday for their expert technical assistance and Professor G Gehring (Sheffield University), Dr S Hayden (Bristol University) and Dr G G Lonzarich (Cambridge University) for their encouragement and comments.

References

[1] Stafström, Salaneck W R, Inganäs O and Hjertberg T (ed) 1993 *Proc. Int. Conf. on Science and Technology of Synthetic Metals (Göteborg, 1992)*; *Synth. Met.* **55–7**
Heeger A J (ed) 1993 *Proc. Conf. European MRS (Strasbourg, 1993)*; *Synth. Met.* **61**

[2] Urayama H, Yamochi H, Saito G, Nozawa K, Sugano T, Kinoshita M, Sato S, Oshima K, Kawamoto A and Tanaka J 1988 *Chem. Lett.* **1988** 55
Kinoshita N, Takahashi K, Murata K, Tokumoto M and Anzai H 1988 *Solid State Commun.* **67** 465

[3] Schirber J E, Venturini E L, Kini A M, Wang H H, Whitworth J R and Williams J M 1988 *Physica* C **152** 157
Oshima K, Mori T, Inokuchi H, Urayama H, Yamochi H and Saito G 1988 *Synth. Met.* **27** A165
Kang W, Jerome D, Lenoir C and Batail P 1990 *J. Phys.: Condens. Matter* **2** 1665

[4] Parker I D, Friend R H, Kurmoo M, Day P, Lenoir C and Batail P 1989 *J. Phys.: Condens. Matter* **1** 4479
Fujii H, Kajita K, Kawada K, Nishio Y, Kobayashi H, Kobayashi A and Kato R 1993 *Synth. Met.* **55–7** 2939

[5] Williams J M *et al* 1990 *Organic Superconductivity* ed V Z Kresin and W A Little (New York: Plenum)

[6] Sasaki T, Sato H and Toyota N 1991 *Physica* C **185–9** 2687; 1990 *Solid State Commun.* **76** 507

[7] Heidmann C-P, Müller H, Biberacher W, Neumaier K, Probst C, Andres K, Jansen A G M and Joss W 1991 *Synth. Met.* **41–3** 2029
Wosnitza J, Crabtree G W, Wang H H, Geiser U, Williams J M and Carlson K D 1992 *Phys. Rev.* B **45** 3018

[8] Caulfield J, Singleton J, Pratt F L, Doporto M, Lubczynski W, Hayes W, Kurmoo M, Day P, Hendriks P T J and Perenboom J A A J 1993 *Synth. Met.* **61** 63

[9] Shoenberg D 1984 *Magnetic Oscillations in Metals* (Cambridge: Cambridge University Press)

[10] Rahal M, Chasseau D, Gaultier J, Ducasse L, Kurmoo M and Day P unpublished
Chasseau D, Gaultier J, Rahal M, Ducasse L, Kurmoo M and Day P 1991 *Synth. Met.* **41–3** 2039

[11] Doporto M, Pratt F L, Singleton J, Kurmoo M and Hayes W 1992 *Phys. Rev. Lett.* **69** 991

[12] Pippard A B 1965 *Proc. R. Soc.* A **287** 165

[13] Toyota N, Fenton E W, Sasaki T and Tachiki M 1989 *Solid State Commun.* **72** 859

[14] Pratt F L, Singleton J, Kurmoo M, Spermon S J R M, Hayes W and Day P 1990 *The Physics and Chemistry of Organic Superconductors (Springer Proceedings in Physics 51)* ed G Saito and S Kagoshima (Berlin: Springer) p 200

[15] Tamura M, Tajima H, Yakushi K, Kuroda H, Kobayashi A, Kato R and Kobayashi H 1991 *J. Phys. Soc. Japan* **60** 3861

[16] Sugano S, Mori H, Yamochi H and Saito G 1993 *Phys. Rev.* B **47** 14374

[17] Ugawa A, Ojima G, Yakushi K and Kuroda H 1988 *Phys. Rev.* B **38** 5122

[18] Singleton J, Pratt F L, Doporto M, Hayes W, Janssen T J B M, Perenboom J A A J, Kurmoo M and Day P 1992 *Phys. Rev. Lett.* **68** 2500

[19] Quader K F, Bedell K S and Brown G E 1987 *Phys. Rev.* B **36** 156

[20] Mahan G D 1990 *Many Particle Physics* 2nd edn (New York: Plenum)
Leggett A J 1968 *Ann. Phys.* **46** 76

[21] Luttinger J M 1961 *Phys. Rev.* **121** 1251

[22] Hill S, Singleton J, Pratt F L, Doporto M, Hayes W, Janssen T J B M, Perenboom J A A J, Kurmoo M and Day P 1993 *Synth. Met.* **55–7** 2566

[23] Faulhaber J C R, Ko D Y K and Briddon P R 1993 *Synth. Met.* **60** 227
Vlasova R M, Priev S Ya, Semkin V N, Lyubovskaya R N, Zhilyaeva E I, Yagubskii E B and Yartsev V M 1992 *Synth. Met.* **48** 129

Ko D Y K, Briddon P R and Faulhaber J C R private communication
[24] Toyota N 1993 *Proc. Int. Symp. on Superconductivity, (Cairo, 1993)* at press
[25] Ishiguro T and Yamaji K (ed) 1990 *Organic Superconductors* (Berlin: Springer)
[26] Oshima K, Araki K, Yamazaki H, Kato K, Maruyama Y, Yakushi K, Mori T, Inokuchi H, Mori H and Tanaka S 1991 *Physica* C **185–9** 2689
[27] Oshima K, Yamazaki H, Kato K, Maruyama Y, Kato R, Kobayashi A and Kobayashi H 1993 *Synth. Met.* **55–7** 2334
[28] Caulfield J M 1994 *DPhil Thesis* University of Oxford
[29] Andraka B, Kim J S, Stewart G R, Carlson K D, Wang H and Williams J M 1989 *Phys. Rev.* B 40 11 345
[30] Brinkman W F and Rice T M 1970 *Phys. Rev.* B 2 4302